ACTA METALLURGICA SLOVACA
2020, VOL. 26, NO. 4, 166-177

RESEARCH PAPER

INVESTIGATION OF DISTINCTIVE SOLUTIONIZING PROCESS PARAMETERS ON SIGNIFICANTLY INCREASING IN STRENGTH AND DUCTILITY OF As-CAST AZ80 Mg ALLOY

Mui Kheng Yeoh [1,2], XingHe Tan [1], Richard Wai Onn Kwok [3], Teik-Cheng Lim [2]*

[1]ST Engineering Land Systems Ltd, 249 Jalan Boon Lay, Singapore 619523

[2]School of Science and Technology, Singapore University of Social Sciences, 463 Clementi Road, Singapore 599494

[3]SMRT Corporation Ltd, 251 North Bridge Road, Singapore 179102

* Corresponding Authors: yeohmk@stengg.com, tel: +6568640721, School of Science and Technology, Singapore University of Social Sciences, 463 Clementi Road, Singapore 599494

Received: 24.10.2020
Accepted: 18.11.2020

ABSTRACT

A distinctive solutionizing process parameter was developed and performed to significantly enhance strength and ductility of aged AZ80 Mg alloy. The microstructure-processing-properties relationship was studied to help elucidate the mechanism. Microstructure and mechanical properties were studied by using optical microscopy, Field Emission Scanning Electron Microscopy, Transmission Electron Microscopy, X-ray diffraction, hardness and tensile testing. The results show that the solutionization at 380°C/10h followed by 420°C/10h promoted significant dissolution of eutectic $Mg_{17}Al_{12}$ and intermetallic phases. After standard aging at 200°C/10h, the formation of high-density precipitates $Mg_{17}Al_{12}$ with more spheroidization precipitates and lesser discontinuous precipitates morphology, which was not observed in conventional heat treatment for aged AZ80 Mg alloy. Fine precipitates $Mg_{17}Al_{12}$ resulted in a significant increase in ultimate tensile strength (50.3%), yield strength (35%), elongation (106%) and hardness (40%) compared to conventional heat treated cast AZ80 Mg alloy. These properties are comparable to the commonly used aerospace grade cast aluminium alloy A356.

Keywords: Cast AZ80 Mg alloy, Heat Treatment, Annealing Twins, Solutionizing, Strength, Ductility

1. INTRODUCTION

In today's market, demand for cast magnesium (Mg) alloys is considered one of the largest and fastest-growing due to their wide usage and application. In addition to the aerospace and automotive industries, demand for cast Mg alloys has been growing in the biomedical and military industries as well. The key factor for the increase in demand is their superior castability with a good combination of mechanical performance and lightness. Among the commercial cast Mg alloys, Mg-Al-Zn alloys have been widely used in many industrial sectors and defense industries owing to their attractive high specific strength to weight ratio and low cost. Nevertheless, cast AZ80 Mg alloy has relatively low strength and ductility and is restricted in its applications as compared with other cast alloys.

In order to increase uptake of cast AZ80 Mg alloy in the commercial markets, efforts have been directed towards development of materials through new processing techniques, alloying of elements and grain refinement. Recent research has shown increasing interest in enhancing the strength of cast AZ80 Mg alloy by the addition of nano-composites to create particulate reinforcements in a matrix of alloy [1-3]. Also, there has been greater focus on improving the mechanical properties of cast AZ80 Mg alloy with equal-channel angular pressing for grain refining prior to aging treatment [4, 5]. In addition, researchers have been trying to enhance the strengthening effect through micro-alloying elements such as Lithium [6], Yttrium [7], Neodymium [8], and Cerium [9] etc. Even though those processes can strengthen the properties of the material with good results, their production costs are comparatively higher and cycle time is longer. This has driven efforts to achieve strength enhancement through various heat treatment processes in order to expand its applications. In the past, many researchers focused their studies to develop and optimize heat treatment processes to achieve the desired mechanical properties of wrought AZ80 Mg alloy [10-13]. Only some investigations have been reported that relate to microstructure evolution and mechanical properties through heat treatment of as-cast AZ80 Mg alloy condition [14-17]. However, the strengthening effects reported in those studies are rather limited. In particular, Zhang et al. [15] studied heat treatment effects on the mechanical properties of cast AZ80 Mg alloy and achieved a tensile strength of 196-197 MPa and yield strength of 126-129 MPa, but ductility (3.66-4.42%) is still relatively low after aging. Besides, several researchers [14, 17] have suggested that it is possible to achieve good mechanical properties by controlling the microstructure, texture, dissolution of β-$Mg_{17}Al_{12}$ phase etc. through optimization of solution treatment. However, it is still difficult to achieve a good combination of strength and ductility, which may restrict their usage and application. More recently, several studies have been devoted to the development of better mechanical performance in as-cast AZ80 with different solutionizing times to enhance the dissolu-

tion of the eutectic $Mg_{17}Al_{12}$ phase [18, 19]. The findings suggest that the dissolution of β-$Mg_{17}Al_{12}$ phase is highly time and temperature dependent. The volume fraction of the β-$Mg_{17}Al_{12}$ phase decreased with time and temperature. These second-phase particles have been found to affect the mechanical properties of magnesium alloys [16, 18-20]. Although the results show significant differences in tensile properties, ductility is still a concern, which seem to be insufficient for high performance industrial applications. Therefore, significant efforts are still needed to develop a good combination of strength and ductility on as-cast AZ80 Mg alloy.

The dissolution of the β-$Mg_{17}Al_{12}$ phase has been reported to dissolve effectively into the matrix with the development of a two-step solution treatment method compared to a single step in some magnesium alloys [21-23]. This resulted in a better precipitation strengthening effect after subsequent aging. However, those suggested solution treating schedule may not be suitable for certain magnesium alloys although they are from the same alloy classes. By changing the heat treatment times and temperatures, the mechanical properties of different magnesium alloys can vary widely. Also, mechanical properties can be adversely affected by an increase in solution temperature or prolonging of solutionizing time. Hence, further modification of these heat treatments is required to develop for cast AZ80 Mg alloy in order to obtain the most desirable combination of properties.

To improve on what has been achieved by the research aforementioned, a distinctive solutionizing process parameter was developed and performed on as-cast AZ80 Mg alloy. The aim of this work is to investigate the effects of the solutionizing parameter and its age hardening response. Also, to elucidate the effects of dissolution of β-$Mg_{17}Al_{12}$ phase during solutionizing on enhancing the strength hardening effects leading to better mechanical properties of cast AZ80 Mg alloy. The relationship of precipitate morphology, mechanical properties and fracture failure mechanism of cast AZ80 Mg alloy is discussed.

2. MATERIAL AND METHODS

The commercial as-cast AZ80Mg alloy supplied ingot form was used in this study. The chemical composition of the as-cast AZ80 Mg alloy was determined by the inductively coupled plasma-AES method and its nominal composition by Mg-8.15Al-0.52Zn-0.20Mn (in wt.%). Prior to the solutionizing process, the as-cast AZ80 Mg specimens were homogenized at 300° C for 10 h at a heating rate of 1°C/min, followed by air cooled to reduce the segregation due to the casting solidification process and to obtain a better homogeneous microstructure. In order to investigate the effect of homogenization temperature on the microstructure, another homogenization at 380°C for 10 h (at heating rate of 1°C/min) with air cooling was studied to establish optimum homogenization conditions that would affect the subsequent solutionizing process.

The optimum homogenization conditions that have been established for the best microstructure will be selected and subjected to the subsequent solutionizing process. During the solutionizing process, a protective atmosphere with argon gas was used in the furnace for surface protection. In order to prevent fusion of eutectic compounds and voids formation [24], the specimens were loaded into the furnace at 260°C and heated to 420°C at a heating rate of 1°C/min, followed by holding at 420°C for 10 h and immediately quenched in water at room temperature (T4). Subsequently, aging treatment at 200°C for 10 h was applied on the solutionized specimens to study the effect of microstructure and mechanical properties in the as aged condition (T6). In this study, a distinctive solutionizing process (homogenization follow by solutionization) was denoted as T4X and denoted as T6X when inclusive of the ageing process. Figure 1 shows the schematic diagram of the entire heat treatment cycles that were carried out in this study.

To study the difference in microstructural morphology between as cast and heat treated AZ80 Mg alloy specimens, optical microscope (OM) and field emission scanning microscope (FESEM) equipped with energy dispersive spectrometer (EDS) were used to carry out microstructural characterization. For phase identification, X-ray diffraction using CuK_α radiation (k = 1.5406 A°) and a scan speed of 2°/min was conducted. Using Match! Software for XRD phase identification, the volume fraction V_f of the β-$Mg_{17}Al_{12}$ phase was measured. Metallographic specimens were prepared in accordance with ASTM E3-11, by first cross-sectioning, cold mounting, grinding and polishing. After obtaining a scratch free surface, specimens were etched with one of the following etchants to reveal their microstructures: acetic-glycol (20 mL acetic acid, 1 mL HNO_3, 60 mL ethylene glycol, 20 mL H_2O), acetic-picral (10 mL acetic acid, 4.2 g picric acid, 10 mL H_2O, 70 mL ethanol) and phosphor-picral (0.7 mL H_3PO_4, 5 g picric acid, 100 mL ethanol) [25]. Selection of etchants is dependent on the material condition of specimens. Quantitative analyses of the grain size and various phases were performed with Olympus Stream Image Analysis Software. The average grain size measurements were made using the linear intercept method in accordance with ASTM E112-13. TEM studies were also conducted using a combination of bright field (BF) and dark field (DF) TEM imaging, selected area electron diffraction (SAED). TEM was conducted on a JEM 2010F (JEOL) with an accelerated voltage of 200 kV. The TEM specimens were prepared by cross-sectioning them into thin slices of approximately 200µm thick and mechanically polished to thin foils of less than 30µm thick. Foils were then punched out with a disk punch to 3 mm diameter disks. They were subjected to ion milling thinning with a Gatan Precision Ion Polishing System (model 691) under operating conditions of 5.0 kV and an incident angle of 4-6° to a perforation thickness of less than 20µm. The perforations had been cleaned with ethanol after ion milling thinning.

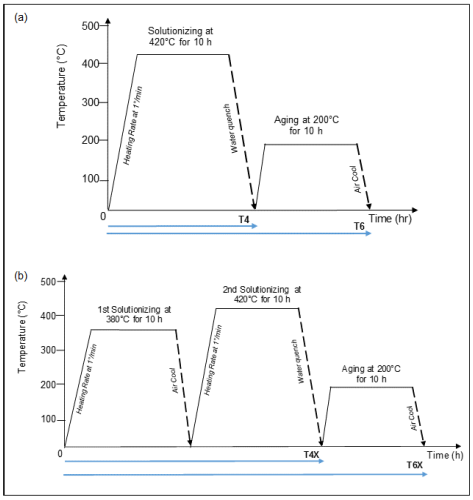

Fig. 1 Schematic diagram of the entire heat treatment cycles for (a) conventional heat treatment (T6); (b) current heat treatment (T6X) with two-step solutionizing and aging

Tensile tests were conducted at ambient temperature with a universal testing machine (Instron Model 8801) using a tensile speed of 0.5mm per minute in accordance with ASTM B557-15. After removal of the extensometer, speed was increased to 3mm per minute. A minimum of 3 specimens for each condition were

tested. SEM fractography was also performed on the fracture surface of the tensile test specimens. Vickers microhardness testing with 100g load applied and 15 seconds of holding time was performed on cross-sectioned and polished specimens in accordance with ASTM E384-17 using Matsuzawa microhardness tester MMT-X7. To ensure result reliability, 10 indentations were measured on each specimen.

3. RESULTS AND DISCUSSION

3.1 Heat Treatment Process

3.1.1 Homogenization at 300°C or 380°C

Homogenization treatment helps to increase the uniformity of the material by eliminating composition segregation, non-equilibrium phases and stresses induced during casting solidification. Studies showed that homogenization treatment can effectively improve microstructure uniformity and distribution of the $Mg_{17}Al_{12}$ phase, as well as enhance mechanical properties of magnesium alloys [26,27]. In order to improve the uniformity of microstructure, the as-cast AZ80 Mg alloy specimens were first homogenized at 300°C for 10 h followed by air cooled. A comparative study with homogenization at 380°C for 10 h with cooled air was conducted to determine the optimal homogenization temperature prior to solution treatment. The typical microstructure of AZ80 magnesium alloy in the as-cast condition and a microstructural comparison of dissolution of secondary phases in different temperatures are shown in Fig. 2. It can clearly be observed that dissolution of β-$Mg_{17}Al_{12}$ phase and eutectic α+β phase had occurred. Microstructures with dendritic arm segregation formed during the solidification process and discontinuous precipitation or lamellar eutectic α+β phase are clearly visible in the as-cast condition as shown in Fig. 2(a) and (b). At 300°C, the network β-$Mg_{17}Al_{12}$ phase along the grain boundary was found to have broken down, the thickness of β-$Mg_{17}Al_{12}$ phase was reduced and eutectic α+β phase was also partially dissolved into α-Mg matrix (see Fig. 2c and d). However, at 380°C, the coarse eutectic β-$Mg_{17}Al_{12}$ had clearly further broken down (see Fig. 2e and f). The dendritic structure and eutectic α+β phase entirely disappeared and grain formation could be observed. Also, the vast amount of coarse β-$Mg_{17}Al_{12}$ phase decreased dramatically and this helped to improve the microstructure homogeneity as compared to the as-cast condition. This can be seen consistently with an image analyzer in the area fraction of β-$Mg_{17}Al_{12}$ phase (see Fig. 2g). The area fraction of β-$Mg_{17}Al_{12}$ phase was decreased from 25.6% (as-cast condition) to 21.6% (at 300°C) and 7.3% (at 380°C). This implies that the higher the temperature is, the faster the rate of dissolution of the eutectic $Mg_{17}Al_{12}$ phase and the lower the fraction of β-$Mg_{17}Al_{12}$ phase are expected to be. However, too high a homogenization temperature or that which is above the eutectic should be avoided. Hence, homogenization at 380°C (denoted as 1st solutionizing) is selected as the optimum homogenization temperature to produce the best microstructure.

3.1.2 Solutionizing Process (T4 & T4X)

The selected solutionizing temperature used should be below the eutectic temperature of 437°C to prevent eutectic melting due to over-heating. In this study, as-cast AZ80 Mg alloy was first solutionized at a lower temperature to partially dissolve the eutectic of $Mg_{17}Al_{12}$ and subsequently heated near to the eutectic temperature for better dissolution of undissolved phases. Figure 3 illustrates the evolution of microstructure for as-cast, homogenization, solutionizing condition for T4 and T4X, and their respective area fraction of β phase. As presented in Fig. 3a, the as-cast alloy exhibits a rather inhomogeneous microstructure with coarse eutectic β-$Mg_{17}Al_{12}$ phase network mainly distributed around the grain boundaries. A relatively high proportion of coarse eutectic $Mg_{17}Al_{12}$ phase had clearly dissolved in α-Mg matrix after homogenization at 380°C for 10 h (Fig. 3b). Also, it can be seen that a fine β phase network is still segregated in the small remaining grain boundaries. In addition, the interdendritic structure was still observed to be segregated at the grain boundaries in T4 (Fig. 3c) as compared to T4X (Fig. 3d). This showed an increase in solute solubility for T4X and suggests a supersaturated of grains formation.

Moreover, from Fig. 3e and f, it were observed that there is a significant reduction in area fraction of β-$Mg_{17}Al_{12}$ phase after T4X. The amount of the dissolution of β-$Mg_{17}Al_{12}$ phase varies dramatically from 2.86% to 0.16% in the microstructure after T4 (Fig. 3e) and T4X (Fig. 3f), respectively. This implies that T4X could further improve the homogenization of microstructure, promote dissolution of eutectic phases and increase solute diffusion into the matrix while maintaining a stable grain microstructure. Further, the corresponding SEM images in Fig. 3g and h show that some insoluble particles are observed at grain interiors. These chunky, irregular shaped particles are identified by EDS as Al-Mn intermetallic compounds which are formed during solution treatment when traces of manganese and aluminium are present. This suggests that the intermetallic compound of Al-Mn was not significantly dissolved during solutionizing at 420°C. These results are in agreement with the findings of Braszczyńska-Malik [28] who reported that only the intermetallic compound Al_8Mn_5 did not undergo any notable changes after heat treatment.

After solutionizing, the grain size increased slightly as compared to as-cast specimens (see Table 1). The average grain size was increased from as-cast condition 91µm to 127µm (T4) and 111µm (T4X). This showed that the T4X involving an additional 10 h of soak time was supposed to lead to growth in grain size but in this case, it was still capable of maintaining a smaller grain size even though the soak time was longer. A complete dissolution of secondary phases occurred in T4X, followed by nucleation when grain growth stagnated. The smaller grains began to develop inside the larger grains and thus the finer grains were observed. The finer grains may be attributed from maximum solubility of solute elements that resulted from a supersaturated solid solution. With the maximum solubility of solute, the mobility of boundaries may be restricted and against the grain growth. Most research efforts studied were focused on explaining the solute content and the grain microstructure during casting solidification process in Mg-Al alloys [29-32]. In particular, Cáceres et al. [33] studied the solid solution strengthening on Mg-Al alloys and demonstrated that there is correlation between the solute Al content and the grain size, i.e. 8% Al more favorably to achieve a finer grain size of 95µm, which is in good agreement with current work. However, the effects of $Mg_{17}Al_{12}$ phase solubility on morphology during solution treatment were not clearly discussed in those studies. Another factor that contributed to the finer grain size could be due to formation of annealing twins during solutionizing process. It is interesting to observe from microstructural studies that multiple twinning variants are formed after solutionizing in T4, as shown in Fig. 4 (a) and (b). The variants appeared as both parallel lines and lenticular shape. Likewise, multiple twinning was observed in Fig. 4(c) and (d). In contrast, T4X induced more twinning as compared to T4 and has a more complicated microstructure with more complex morphology and texture. Also, T4X which is being susceptible to multiple twins formation, yielding better control in grain size stability. It is well known that pure magnesium and its alloys exhibit twinning after deformation by mechanical processing such as extrusion, compression, rolling etc. It can be identified as a type of twinning caused by deformation and annealing. However, most research works [34-37] have focused

on reporting the effect of deformation twins on AZ80 Mg alloys but limited studies were done on annealing twins. The studies on annealing twins on other cast alloys are rather limited. Figure 4(e) revealed multiples twins from one grain of T4X specimen. This result is in agreement with the findings of Syam Prasad et al. [38] and Jia Hongmin et al.[39] on ZE41 and Mg-4Zn alloys respectively, they consistently reported that thermally induced twins were observed in cast Mg alloy after solutionizing. The twin formations observed in this study are considered annealing twins. The annealing twins or transformation twins formed are caused by changes in the normal growth mechanism and phases during crystal transformation [40] Comparatively, T4X has a more complicated microstructure with more complex morphology. In this research work, the lenticular like lens shape twinning formed without being subjected to any mechanical deformation process. Lenticular shape twinning is usually formed during plastic deformation. According to literature, such formation of twinning could occur during the solid phase transformation or casting solidification process [40,41]. The initial homogenization process at 380°C for 10 h help improve the dissolution of $Mg_{17}Al_{12}$ eutectic structure and increase the solid solubility of Zn and Al in α-Mg matrix in the process. During the subsequent solutionizing at a higher temperature of 420°C for 10 h, recrystallization could occur in some grains and twin formation with parallel line occurred in association with grain growth. The mechanism for the formation of multiple annealing twins in T4X can be attributed to higher solute solubility in the matrix and the stored energy after homogenization providing a greater driving force for recrystallization [40]. This is also likely to promote the formation of stable fine grain sizes during the subsequent aging process. The experiment results indicate that T4X is susceptible to twin formation. It shows convincing evidence that the presence of twin formation is influenced by the development of texture of the solutionized condition, leading to stable grain size and finally enhancing the yield strength. This study revealed that twinning was suppressed after aging, and this led to a strong evolution of the aging texture. As a consequences, increase in strengthening effect on cast AZ80 Mg alloy.

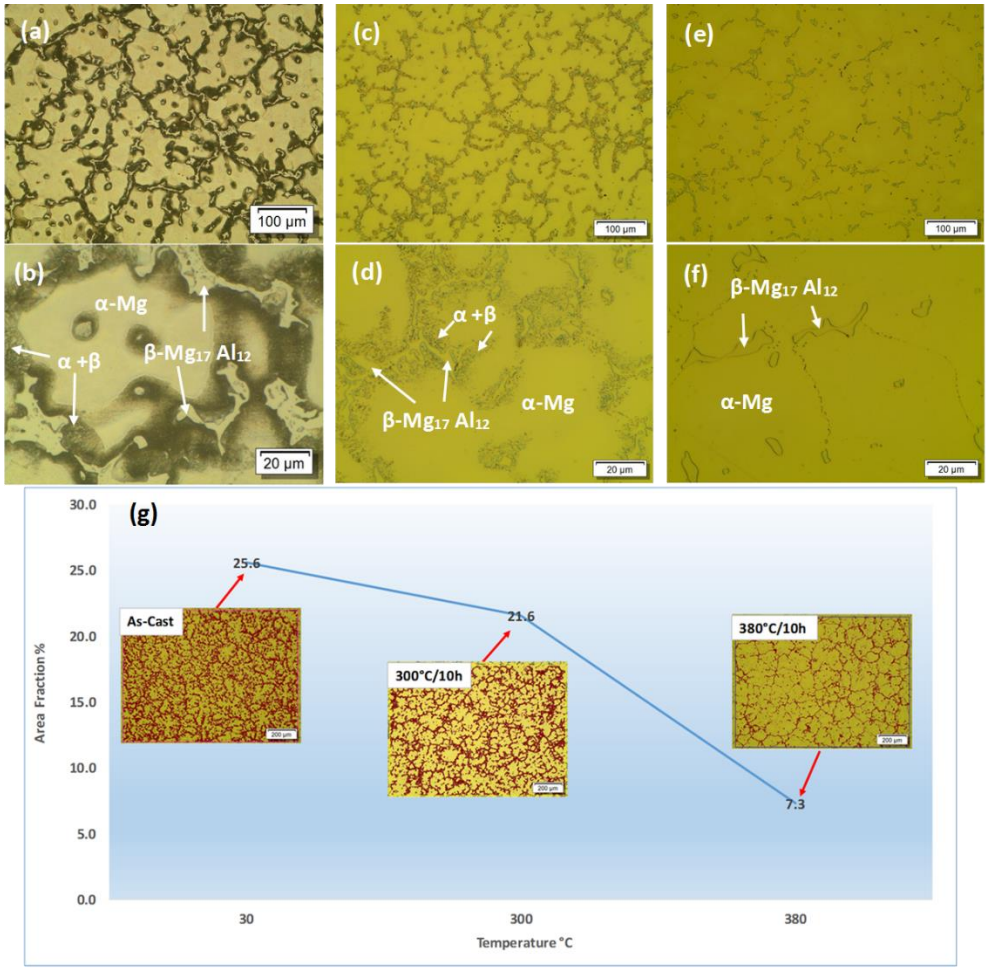

Fig. 2 Microstructure of AZ80 Mg alloy with OM (a)-(b) as-cast condition; (c)-(d) after homogenization at 300°C/10hours; (e)-(f) after homogenization at 380°C/10hours; (g) Effect of temperature on area fraction of β phase

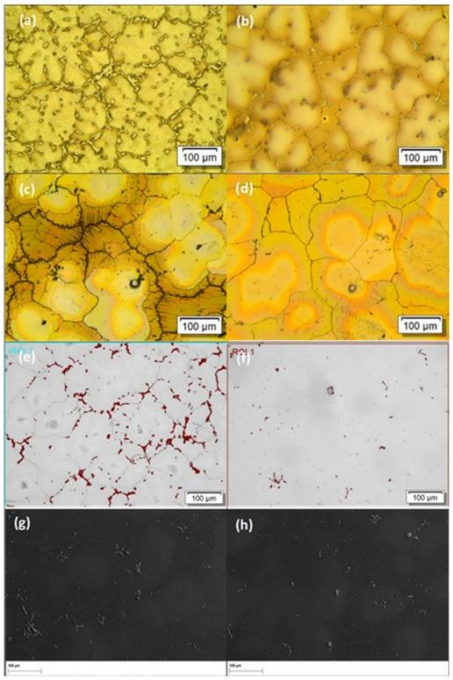

Fig. 3 Microstructure for (a) as-cast; (b) homogenized at 380°C; (c), solutionizing at 420/10 h with water quench (T4); (d) two-step solutionizing (T4X); (e) area fraction for T4 $F_A\beta$ = 2.86%; (f) area fraction for T4X $F_A\beta$ = 0.16%; (g) SEM image for T4; (h) SEM image for T4X

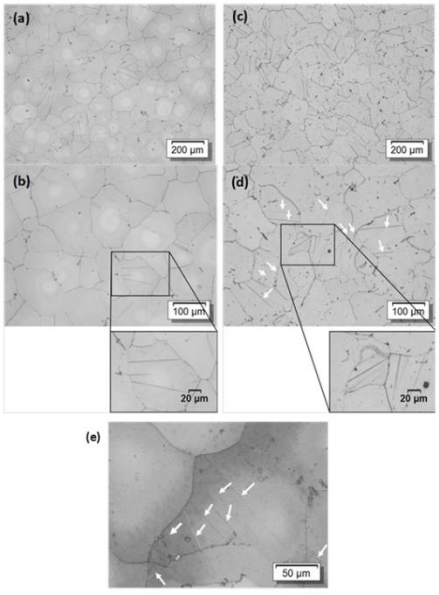

Fig. 4 Optical micrograph showing twinning formation in (a)-(b) T4 condition; (c)-(d) T4X condition; (e) multiples twins in a grain of T4X. Twins are labelled with arrows

Table 1 Grain size measurement and volume fraction ($Mg_{17}Al_{12}$) for HT Conditions

HT Conditions	Specimen ID	Average Grain Size (µm)	Volume Fraction % of $Mg_{17}Al_{12}$
F	As Cast	90.69±1.07	11
T4	S10WQ	127.25±7.10	2
T4X	SS10WQ	111.41±4.92	1
T6	S10WQ-A10	99.00±3.41	16
T6X	SS10WQ-A10	91.00±2.89	11

3.1.3 Solutionizing with aging (T6 & T6X)

SEM image as shown in Fig. 5 revealed that T6 and T6X condition developed with variations in precipitation morphology. The microstructure in as aged condition is generally characterized by the formation of continuous precipitates (CP) and discontinuous precipitates (DP). The nucleation for these two types of precipitates were shown to grow differently. Both types of precipitates occurred competitively and simultaneously. The precipitate morphology of the β-phase in Mg-Al is highly dependent on the temperature and soak time [42,43]. It is noticed that T6 (Fig. 5a) resulted in the formation of distinct DP and dominant morphology. Figure 5b show the formation of the DP with lamellar structures and the CP finely distributed in an orderly parallel manner. CP grows within the parent grain whereas discontinuous precipitate grows at grain boundaries. The CP as presented in Fig. 5c appeared to be lath shaped with long and short lengths, in a specific orientation with respect to the habit plane and matrix. However, a higher area fraction of fine CP is observed in T6X (Fig. 5d). The CP of lath structure for T6 and T6X constituted about 30-40% and 60-70% of area fraction, respectively.

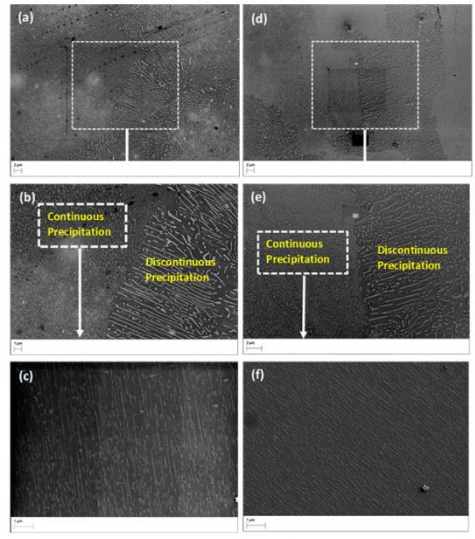

Fig. 5 SEM Micrograph showing DP and CP with different heat treatment: (a)-(c) T6 condition; (d)-(f) T6X condition

In this research work, it was observed that the CP were dominant as compared to DP in T6X. It can be attributed to the increase in supersaturated solid solution and twins formation that accelerates the formation of higher amounts of CP. The result is in

agreement with K.N. Braszcyńska-Malik [44] who reported that the twins boundary constitute favorable to form continuous precipitates after annealing of cast AZ91. The development of CP is important as the mechanical properties are highly dependent on its volume fraction. In Fig. 5(f), fine and thin lath shapes of CP are observed in SEM images of T6X. Also, the CP of T6X was observed to be denser as compared to T6.

In addition, it is known that the discontinuous precipitation reaction is characterized by a discontinuous change in orientation and composition between the matrix and across the migration boundary [45]. The DP nucleate and grow at the grain boundaries in the parent phase due to the relatively high energy that is a result of dislocations and defects [15]. With higher magnification as shown in Fig. 6a, SEM examination revealed clearly the DP at grain boundary growing behind a migration reaction front (RF). Its growth rate is dependent on volume diffusion of the solute in the matrix phase [46]. When the DP grow, the grain boundary was carried along with them. Besides the irregular shape of the lamellar structure, there were globular precipitates found surrounding the lamellar as shown in Fig. 6(b). This could be due to the spheroidization process, in which the partially lamellar structures break down into discrete precipitates. The occurrence of this reaction influences the changes in precipitate morphology. Figure 6(c) and (d) show a large volume of smaller globular formation with irregular slab structures observed in the DP region of T6X specimen. This shows that T6X leads to more fragmentation and spheroidite formation. There were more spherical shaped, discontinuous precipitates with thinner and shorter length, as well as more breakdowns of lamellar and globular precipitates at the grain boundaries. It was also observed that there was a lesser formation of lamellar with shorter length and width. The growth of DP was greatly reduced, though not completely suppressed. Similar to the T6, the T6X microstructure shows that there was a different orientation relationship between the precipitation habit plane and matrix [45]. Manna et al. [47] reported that the morphology of discontinuous precipitation is usually in lamellar structure, sometimes fibrous shaped and very seldom in a globular form. However, the current study showed theformation of larger amounts of globular structures instead of lamellar structures, indicating that T6X would enhance ductility. The presence of globular precipitates results in improvements in plasticity whereas lamellar precipitate decrease plastic properties of the alloys [48].

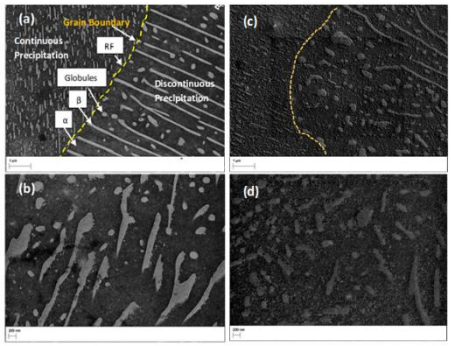

Fig. 6 The precipitate microstructure of AZ80 alloy with processes (a)-(b) T6 condition with long and wider discontinuous precipitates; (c)-(d) T6X condition with spherical shape and shorter discontinuous precipitate

Besides, TEM investigation was performed and revealed the growth of continuous precipitate particles with different morphology for T6 and T6X. Figure 7 showing TEM images with bright field imaging clearly showing the morphology and distribution of β precipitates in T6 and T6 specimens. The precipitates in both specimens appeared in lath shape with their habit planes and grow along a direction a parallel to the basal plane of the matrix $(0001)_\alpha$ and with small amount of lens-shaped precipitates are lying in the basal plane. These precipitates are reported with the predominant of Burger OR with the matrix [43,49,50]. In T6 specimen as shown in Fig. 7a, less precipitates particles had been formed in the Mg matrix as compared to Fig. 7b (T6X). Under the higher magnification (see Fig. 7c and d), it could be seen that most precipitates had shorter lengths, larger interparticle spacing distance and formed in small volume fractions in Fig. 7c. The sizes of precipitates were 17-47nm in width. In contrast, precipitates in Fig. 7d (T6X) had grown to their maximum length and are thin & long, lath shaped and with a larger aspect ratio as compared to Fig. 7c (T6). Their particle sizes were reduced to 13-30nm width morphology (Table 2). A few precipitates were short and lath shaped. More precipitates with the lath-shaped precipitates were dominated, the volume fraction and number density of precipitates are increases as well. Comparison with literature, the precipitates in T6 and T6X specimens were found to be much smaller in size (refer to Fig. 7e for ease of reference). In addition, the interparticle spacing measured are significantly reduced for T6X specimen with an average of 40nm and that will influence on the strength. This implies that T6X has better ability to produce fine dispersion of precipitates with smaller the interparticle spacing and that could further resist the dislocation movement and improved strength of this alloy. Table 2 shows the summary results of the measured particle size and interparticle spacing for both T6 and T6X specimens. Generally, the width and length of the precipitate in the T6X specimen was determined to be shorter than the T6 specimen. However, some longer length of precipitates still were observed in T6X specimen. As reported by Celotto [43], the lath had grown to the maximum length with no significant change in thickness when the maximum hardness is achieved. In this study, precipitates that were thinner in size could be due to longer soak times during T6X that resulted in changes in the morphology of the continuous precipitates.

Table 2 Particle size and interparticle spacing for representative specimens of T6 & T6X

HT Condition	Particle Size		Inter-Particle spacing (nm)	Hardness ($HV_{0.1}$)
	Width (nm)	Length (nm)		
T6	17 - 47	173 - 253	143-331	83.5
T6X	13 – 30	132 - 479	30-121	86.0

In addition, formation of greater amount of precipitates finely dispersed and with moiré fringes contrast were observed in T6X specimen, as illustrated in Fig. 8a (T6X). More dislocations appearing as curved dark lines running through the precipitates are lying primarily in the basal plane of T6X specimen as shown in Fig. 8b and c. It is clearly observed that some precipitates are bypass dislocation lines and this interaction could cause the climbed or bowed out between the precipitates by Orowan mechanism for strong obstacles. Also, most precipitates appear to be distributed on or near dislocation lines, and this dislocation is more favorable to the formation of a precipitate nucleation site. Besides, moiré pattern contrast showed dislocation-precipitate particles interaction at both ends and dislocation gliding was observed due to precipitate overlap. It also appears from the center of precipitate particles. This dislocation gliding in the matrix is not capable of cutting through those precipitates which act as strong obstacles for greater strengthening effect [52]. The

hardness of β-$Mg_{17}Al_{12}$ is much higher than α-Mg matrix. This observation further demonstrated that the T6X specimens produced strong precipitate particles that effectively hinder dislocation movements and resulted in a better age-hardening response compared to the T6 specimen, which is also in good agreement with the measured tensile results.

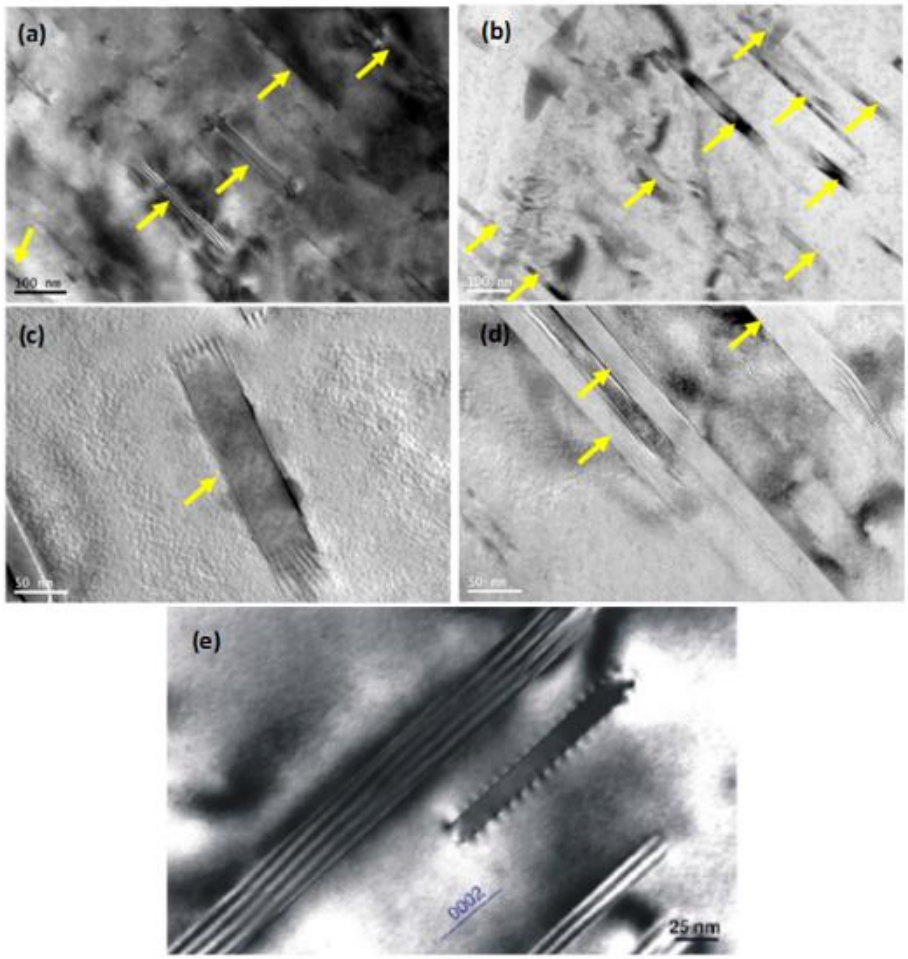

Fig. 7 TEM images showing lath-shaped precipitate morphology for (a)–(b) T6 condition; (c)–(d) T6X condition; (e) AZ91 after aged sample for ease of reference, source adapted from Ref.[51]. Precipitates are labelled with yellow arrow

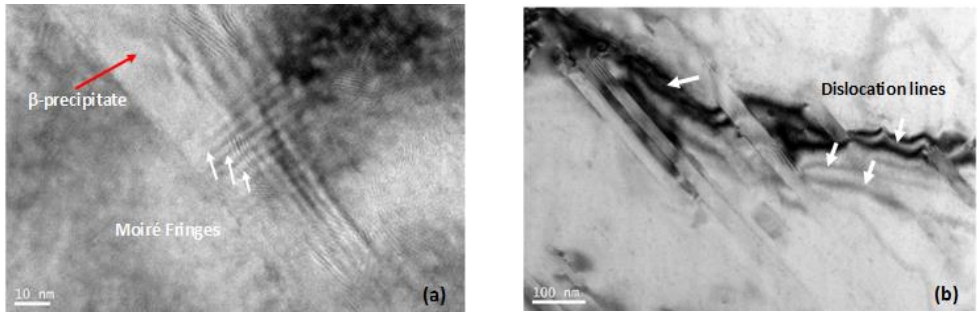

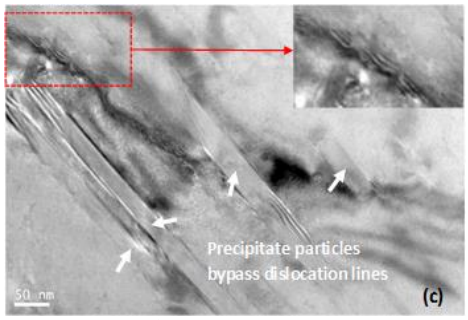

Fig. 8 TEM image for T6X condition showing (a) multiples overlapping of precipitates and with strong moirè patterns contrast (precipitates with white arrow); (b) dark curves showing the dislocation lines with dislocation bypass precipitate particles; (d) enlarge the image from (b)

Under the dark field images, the selected area electron diffraction (SAED) patterns showed that all precipitates particles as analyzed are identified as $Mg_{17}Al_{12}$ particles. TEM dark field image and corresponding diffraction pattern of T6 specimen and T6X specimen are illustrated in Fig.9a and c, respectively. SAED pattern shows the single crystals present in T6 specimen (see Fig. 9b) with diffraction spots that indexing (needs rephrasing) to be Mg. In contrast, ring diffraction patterns were observed for T6X (see Fig. 9d) due to multiple crystals. It was produced by diffraction from the polycrystalline Mg alloy which make-up of many tiny single crystals. Those precipitates are from different planes and within randomly orientated crystals. Evidence of Debye ring pattern formation in SAED showed that T6X condition is capable of attaining precipitate density with higher numbers compared to T6. From the diffraction rings obtained, the type of crystal structure and the lattice parameters is identified as fine $Mg_{17}Al_{12}$ precipitates. There is not possible to determine the orientation of a polycrystalline Mg, since there is no single orientation and flipping or turning the polycrystalline Mg will yield the same ring pattern. As for those diffraction spots, it was identified as Mg. However, further with the evidence of the diffraction ring pattern for detected on T6X specimen proved that the large formation of precipitates colonies with this process that changed of the morphology and produced a strong texture of microstructure.

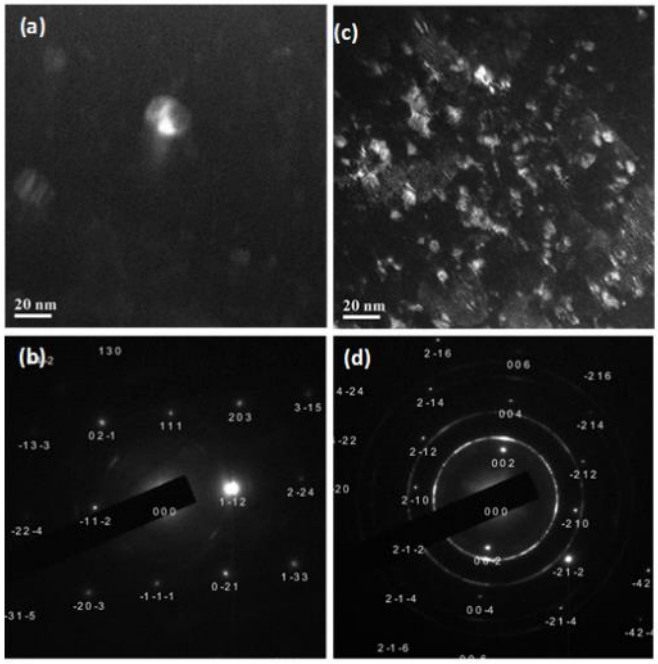

Fig. 9 TEM with dark field imaging showing distribution of precipitates for (a-b) diffraction spot and diffraction pattern corresponding for T6 specimen, (c-d) diffraction spot and diffraction pattern corresponding for T6X specimen

Under XRD analysis, there were no signs of β-$Mg_{17}Al_{12}$ phase for solution treated condition at T4 and T4X as shown in Fig. 10a. The XRD results further confirmed the dissolution of β-$Mg_{17}Al_{12}$ phase, these were consistent with the metallographic observations. However, the β-$Mg_{17}Al_{12}$ phase reappeared after aging, where its diffraction pattern was observed for T6 and T6X. The β-$Mg_{17}Al_{12}$ phase was found to have precipitated from the supersaturated solid solution and formed disperse precipitates. Also, it can be clearly observed that β-$Mg_{17}Al_{12}$ phase diffraction peak had less formation of $Mg_{17}Al_{12}$ for T6X specimen. Both enlargement spectrums shown in Fig. 10(b) indicated higher concentrations of β-$Mg_{17}Al_{12}$ phase. The result was consistent with the quantitative XRD analysis, in which the measured volume fraction was 11 and 16wt% of β-$Mg_{17}Al_{12}$ phase for T6X specimen and T6 specimen respectively (see Table 1). It is well known that as the $Mg_{17}Al_{12}$ content decreases, the ductility increases due to the brittleness of $Mg_{17}Al_{12}$ [53]. Hence, the evidence of presented results indicates that the lower volume fraction in T6X could lead to enhanced ductility.

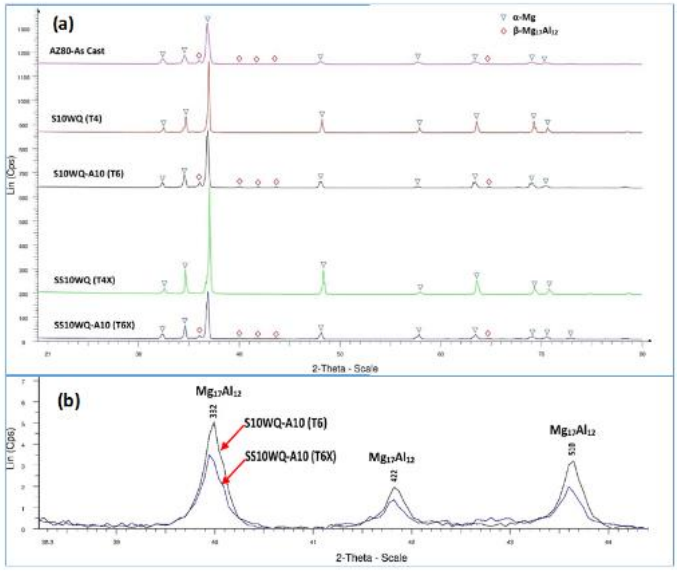

Fig. 10 Comparison on X-ray diffraction patterns of AZ80 in (a) As-cast, T4, T4X, T6 & T6X specimens; (b) enlargement of spectrum for T6 and T6X specimens

3.2 Mechanical Characteristics

Figure 11 shows the engineering stress-strain curves for cast AZ80 Mg alloy subjected to T6 and T6X condition. Also, a summary of the mechanical properties of current work at various heat treated conditions compared with published works for cast AZ80 Mg alloy are listed in Table 3. For this study, the UTS did not change significantly for T4X as compared to T4. It is most likely because the material had reached the peak of super-saturated and the effect of any rise in tensile strength is negligible even with the introduction of two-step solution treatment. In comparison to as-cast (106MPa) and solution treated condition, YS dropped almost 14% after T4 (91MPa). This can be attributed to grain growth and reduction in the volume fraction of β-$Mg_{17}Al_{12}$ phase, as shown in Table 1. Also, another contributing factor could be increased interlamellar spacing, which was studied in a previous work [19]. However, it is noticeable that the YS changed slightly in T4X (102MPa). This could be due to the fact that T4X tends to form higher amounts of multiple twins, which accounts for the stable structure and prevents further grain growth.

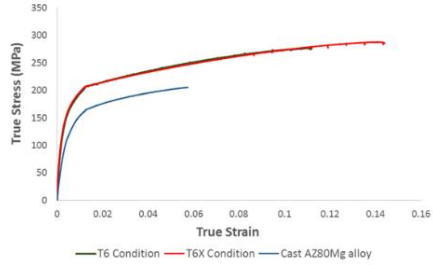

Fig. 11 True stress-strain curve for representative samples of as-cast, T6 and T6X conditions

Table 3 Mechanical Properties of AZ80 Mg alloy for various heat treatment processes

HT Condition	Specimen ID	Tensile Properties			Hardness ($HV_{0.1}$)	Ref.
		UTS (MPa)	YS (MPa)	Elongation (%)		
F	As-Cast	191 ± 1	106 ± 2	6.3 ± 0.3	61.2 ± 2.8	
T4	S10WQ	274 ± 6	91 ± 4	16.0 ± 1.3	64.0 ± 4.1	
T4X	SS10WQ	266 ± 7	102 ± 8	16.0 ± 3.1	63.7 ±2.8	
T6	S10WQ-A10	287 ± 1	156 ± 5	9.0 ± 0.5	83.5 ± 4.5	
T6X	SS10WQ-A10	287 ± 2	143 ± 1	13.0 ± 0.4	86.0 ± 3.0	
T6	Cast AZ80	199.41	126.32	3.66	76.3	Zhang et al. [15]
T6	Cast Al A356	221	152	2		AMS 4218J

After T6X, the yield strength was found to be slightly lower as compared to T6. It was likely caused by the slight grain coarsening in T6X (see Table 1) as compared to T6. An exceptional tensile result show both heat treatment processes achieved almost similar ultimate tensile strength at 287MPa. The tensile strength increased significantly (+50% compared to as-cast) after aging. Also, it was observed that the elongation to failure after T6 and T6X is 9% to 13% respectively. The results show that ductility of T6X increases almost 106% compared to the as cast condition (6.3%). This indicates that T6X contributed

greatly to the achievement of better integrated mechanical properties. This could be due to the T6X enhancing the nucleation rate by breaking down the lamellar into discrete particles. The reason for the combination of high strength and ductility of T6X is mainly attributed to the change in precipitation morphology. This can be explained by the combination of greater degree of supersaturated solution and formation of twinning that impeded the dislocation movement. Also, subsequent aging process (T6X) led to the formation of low volume fractions of $Mg_{17}Al_{12}$ and high volume fractions of CP with high density of precipitates. This can significantly improve strength and ductility simultaneously

After aging, the average hardness value was found to increase by 36-40% as compared to the as-cast condition ($61.2HV_{0.1}$). It reached $83.5HV_{0.1}$ and $86HV_{0.1}$ after aging on test specimens for T6 and T6X respectively. Overall, the hardness of aged AZ80 Mg alloy was higher as compared to the as-cast condition due to the solid solution strengthening effect involving the transformation of the supersaturated solid solution to fine precipitates in the matrix and for precipitation hardening.

In order to investigate the fracture behavior, the tensile fracture specimens were examined with SEM as shown in Fig. 12. The fracture behavior for as-cast condition, T6 and T6X specimens are illustrated in Fig. 12a, b and c, respectively. It can be observed in Fig. 12 b and c that both fracture surfaces for T6 and T6X were found to have many parallel plateaus and ledge morphologies which characterize as mixed cleavage fracture mode with the faceted feature and quasi-cleavage fracture. However, the ductile features appear to be more in T6X as compared to T6 specimen. A large plastic deformation zone was observed in Fig 12(c) as compared to Fig. 12(b). As the size of the plastic deformation zone increases, the mechanism of fracture tends towards ductile tearing which is considered as a more ductile fracture. However, both fracture surfaces were found to have many parallel plateau and ledge morphology which can be characterized as mixed cleavage fracture mode. Quasi-cleavage fracture was also observed. The T6X specimen showed a faceted cleavage fracture with more flat face steps but are less wide as compared to the T6 specimen. Under an enlargement of ductile surface region tensile fractography morphology of as-cast condition, T6 and T6X (see Fig. 12d, e and f), it clearly shows with dimples of different sizes and precipitated particles. It also indicates that T6X (Fig. 12f) exhibited more uniformly distribution of smaller precipitated particles as compared to T6 (Fig. 12e). Large colonies of relatively fine precipitated particles, which were nucleated in dimples, could be attributed to enhance both strength and ductility. During the application of tensile stress, plastic deformation is first initiated in the precipitated particles/Mg matrix interface and that leads to the occurrence of decohesion and microvoids formation. With more precipitated particles, it is enabling higher energy absorption with the grain pullouts and repulsion mechanism (needs rephrasing) and led to larger strain to fracture through the interface and thus, increasing ductility.

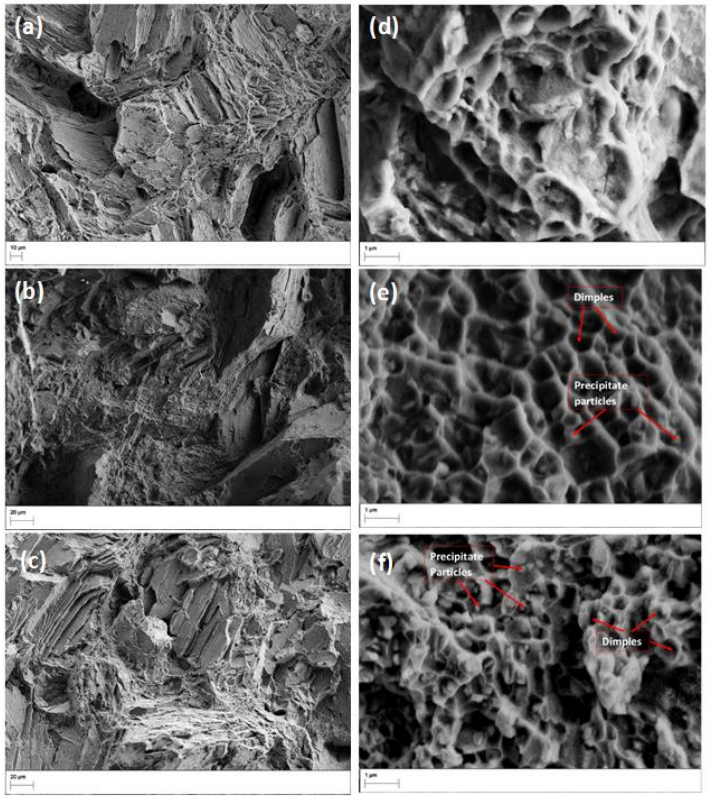

Fig. 12 SEM images showing the variation of appearances of tensile fracture surfaces with ductile features (a-b) as-cast condition; (c-d) T6 condition with large dimples with precipitated particles; (e-f) T6X condition with smaller dimples and a large number of precipitated particles

CONCLUSION

In this study, conventional heat treatment (T6) and current heat treatment (T6X) were performed on the as-cast AZ80 Mg alloy. The following conclusions were made:

- A distinctive solutionizing process was performed at 380°C/10 follow up 420°C/10 and aged at 200h/10h.
- T6X led to more fragmentation and spheroidization with smaller globular precipitates and lesser volume fraction of DP. This resulted in a higher proportion of lath CP dispersed uniformly in the matrix greatly produced an improved combination of mechanical properties. Besides, T6X exhibits more dislocation-precipitate interactions through the Orowan loop mechanism and has produced strong obstacles to dislocation movement. This indicated a better aged-hardening response.
- In addition, Debye ring diffraction pattern was observed for the T6X specimen. The evidence of the diffraction ring pattern proved that large formation of precipitates colonies and with a high number of density produced with this process would contribute to a strong microstructure texture.
- Moreover, tensile fractography studies have shown distinct features for both fracture surfaces of the T6 and T6X specimens. The results of the fractography examination showed that the combination of high ductility and high strength in T6X is due to the presence of large amounts of fine precipitate particles-nucleated in dimples, small dimples in size, decreased interspacing between precipitate and fine precipitate with a large volume fraction.
- The mechanical properties of cast AZ80 Mg alloy with T6X were superior to T6. Significant improvements in a combination of strength and ductility were achieved with increases in UTS (50.3%), YS (35%), elongation (106%) and hardness (40%) as compared with as-cast condition of AZ80 Mg alloy.

Acknowledgements

The authors are grateful for the funding support from ST Engineering Land Systems Ltd. Special thanks to the late Associate Professor Philip Cheang for his great support and encouragement.

REFERENCES

1. Huang SJ, Li CR, Yan KL: Particle reinforcement of magnesium composites SiCp/AZ80 and their mechanical properties after heat treatment. Kovove Materialy 51 (1), 2013, 45-52. https://doi.org/10.4149/km_2013_1_45.
2. Khoshzaban Khosroshahi H, Fereshteh Saniee F, Abedi HR: Mechanical properties improvement of cast AZ80 Mg alloy/nano-particles composite via thermomechanical processing. Materials Science and Engineering A 595, 2014, 284-290. https://doi.org/10.1016/j.msea.2013.12.029.
3. Matin A, Saniee FF, Abedi HR: Microstructure and mechanical properties of Mg/SiC and AZ80/SiC nano-composites fabricated through stir casting method. Materials Science and Engineering A 625, 2015, 81-88. https://doi.org/10.1016/j.msea.2014.11.050.
4. Yin DL, Weng LK, Liu JQ, Wang JT: Investigation of microstructure and strength of AZ80 magnesium alloy by ECAP and aging treatment. Kovove Materialy 49 (1), 2011, 37-42. https://doi.org/10.4149/km-2011-1-37.
5. Tang L, Zhao Y, Islamgaliev R, Valiev R: Enhanced strength and ductility of AZ80 magnesium alloys by spray forming and ECAP techniques, KnE Materials Science, 2016, 168-171. https://doi.org/10.18502/kms.v1i1.580.
6. Wang PC, Lin CC, Huang TY, Lin HC, Lee YH, Yeh MT, Wang JY: Effects of 2 mass % Li addition on the AZ80 Mg alloy. Materials Transactions 49 (5), 2008, 913-917. https://doi.org/10.2320/matertrans.MC200708.
7. Kashefi N, Mahmudi R: The microstructure and impression creep behavior of cast AZ80 magnesium alloy with yttrium additions. Materials and Design 39, 2012, 200-210. https://doi.org/10.1016/j.matdes.2012.02.036.
8. Wang YX, Fu JW, Yang YS: Effect of Nd addition on microstructures and mechanical properties of AZ80 magnesium alloys. Transactions of Nonferrous Metals Society of China (English Edition) 22 (6), 2012, 1322-1328. https://doi.org/10.1016/S1003-6326(11)61321-6.
9. Wei W, Xu C, Zhang J, Cheng W, Niu X: Effects of Ce addition on microstructure, mechanical properties and corrosion resistance of as-cast AZ80 magnesium alloy. China Foundry 11 (3), 2014, 157-162.
10. Uematsu Y, Tokaji K, Matsumoto M: Effect of aging treatment on fatigue behaviour in extruded AZ61 and AZ80 magnesium alloys. Materials Science and Engineering A 517 (1-2), 2009, 138-145. https://doi.org/10.1016/j.msea.2009.03.066.
11. Wu YJ, Zhang ZM, Li BC: Effect of aging on the microstructures and mechanical properties of AZ80 and ZK60 wrought magnesium alloys. Science of Sintering 42 (2), 2010, 161-168. https://doi.org/10.2298/SOS1002161W.
12. Zhu R, Ji W, Wu Y, Cai X, Yu Y: Effect of aging treatment on low-cycle fatigue behavior of extruded Mg-8Al-0.5Zn alloys. Materials & Design 41, 2012, 203-207. https://doi.org/10.1016/j.matdes.2012.05.015.
13. Yu S, Gao Y, Liu C, Han X: Effect of aging temperature on precipitation behavior and mechanical properties of extruded AZ80-Ag alloy. Journal of Alloys and Compounds 646, 2015, 431-436. https://doi.org/10.1016/j.jallcom.2015.06.126.
14. Yakubtsov IA, Diak BJ, Sager CA, Bhattacharya B, MacDonald WD, Niewczas M: Effects of heat treatment on microstructure and tensile deformation of Mg AZ80 alloy at room temperature. Materials Science and Engineering A 496 (1-2), 2008, 247-255. https://doi.org/10.1016/j.msea.2008.05.019.
15. Zhang J, Jiang B, Wang Z, Yuan S, Nan H, Luo H: Influence of aging modes on microstructure and mechanical properties of AZ80 magnesium alloy. China Foundry 4 (4), 2007, 296-299.
16. Kleiner S, Beffort O, Wahlen A, Uggowitzer PJ: Microstructure and mechanical properties of squeeze cast and semi-solid cast Mg-Al alloys. Journal of Light Metals 2 (4), 2002, 277-280. https://doi.org/10.1016/S1471-5317(03)00012-9.
17. Palai P, Prabhu N, Hodgson PD, Kashyap BP: Grain growth and β-$Mg_{17}Al_{12}$ intermetallic phase dissolution during heat treatment and its impact on deformation behavior of AZ80 Mg-alloy. Journal of Materials Engineering and Performance 23 (1), 2014, 77-82. https://doi.org/10.1007/s11665-013-0722-9.
18. Kadali K, Dubey D, Sarvesha R, Kancharla H, Jain J, Mondal K, Singh SS: Dissolution kinetics of $Mg_{17}Al_{12}$ eutectic phase and its effect on corrosion behavior of as-cast AZ80 magnesium alloy. JOM 71, 2019, 2209-2218. https://doi.org/10.1007/s11837-019-03470-3.
19. Yeoh MK, Tan XH, Cheang PHN, Lim TC, Kwok RWO: Effect of solutionizing time on improving the microstructure and mechanical properties of aged AZ80 Mg alloy. Journal of Materials Engineering and Performance 28 (11), 2019, 6836-6852. https://doi.org/10.1007/s11665-019-04382-8.
20. Dini H, Andersson NE, Jarfors AEW: Effect of $Mg_{17}Al_{12}$ fraction on mechanical properties of Mg-9%Al-1%Zn cast alloy. Metals 6 (10), 2016, 251. https://doi.org/10.3390/met6100251.
21. Liang S, Ma Y, Chen R, Han E: Optimization of heat treatment in AZ64 magnesium alloy. Materials Transactions 49 (5), 2008, 986-989. https://doi.org/10.2320/matertrans.MC200756.

22. Shuai D, Feng W, Zhi W, Zheng L, MAO P-l: Enhanced strengthening by two-step progressive solution and aging treatment in AM50-4%(Zn, Y) magnesium alloy. Transactions of Nonferrous Metals Society of China 28 (12), 2018, 2419-2426.
23. Zhang J, Yuan F, Du Y: Enhanced age-strengthening by two-step progressive solution treatment in an Mg-Zn-Al-Re alloy. Materials and Design 52, 2013, 332-336. https://doi.org/10.1016/j.matdes.2013.05.074.
24. *Heat Treating*, Vol 4., ASM International, Ohio, 1991 .
25. *Metallography and Microstructures*, Vol 9, ASM international, Cleveland, 2004.
26. Wu YJ, Zhang BH, Yang YB, Zhang ZM: Effects of homogenizing and extrusion on elongation of as-cast AZ80 magnesium alloy. Advanced Materials Research 626, 2013. https://doi.org/10.4028/www.scientific.net/AMR.626.386.
27. Zheng L, Nie H, Liang W, Wang H, Wang Y: Effect of prehomogenizing treatment on microstructure and mechanical properties of hot-rolled AZ91 magnesium alloys. Journal of Magnesium and Alloys 4 (2), 2016, 115-122. https://doi.org/10.1016/j.jma.2016.04.002.
28. Braszczyńska-Malik KN: Discontinuous and continuous precipitation in magnesium–aluminium type alloys. Journal of Alloys and Compounds 477 (1-2), 2009, 870-876. https://doi.org/10.1016/j.jallcom.2008.11.008.
29. Nagasekhar AV, Easton MA, Cáceres CH: Solute content and the grain microstructure of high pressure diecast magnesium-aluminium alloys. Advanced Engineering Materials 11 (11), 2009, 912-919. https://doi.org/10.1002/adem.200900175.
30. Hou DH, Liang SM, Chen RS, Dong C, Han EH: Effects of Sb content on solidification pathways and grain size of AZ91 magnesium alloy. Acta Metallurgica Sinica (English Letters) 28 (1), 2015, 115-121. https://doi.org/10.1007/s40195-014-0178-4.
31. StJohn DH, Dahle AK, Abbott T, Nave MD, Qian M: *Solidification of cast magnesium alloys*. In: TMS Annual Meeting, 2003, 95-100.
32. Zhang L, Cao Z, Liu Y, Su G, Cheng L: Effect of Al content on the microstructures and mechanical properties of Mg–Al alloys. Materials Science and Engineering: A 508 (1-2), 2009, 129-133. https://doi.org/10.1016/j.msea.2008.12.029.
33. Cáceres CH, Rovera DM: Solid solution strengthening in concentrated Mg-Al alloys. Journal of Light Metals 1 (3), 2001, 151-156. https://doi.org/10.1016/S1471-5317(01)00008-6.
34. Cui Y, Li Y, Wang Z, Ding X, Koizumi Y, Bian H, Lin L, Chiba A: Impact of solute elements on detwinning in magnesium and its alloys. International Journal of Plasticity 91, 2017, 134-159. https://doi.org/10.1016/j.ijplas.2016.09.014.
35. Jain J, Poole WJ, Sinclair CW: The deformation behaviour of the magnesium alloy AZ80 at 77 and 293K. Materials Science and Engineering A 547, 2012, 128-137. https://doi.org/10.1016/j.msea.2012.04.003
36. Jain J, Zou J, Sinclair CW, Poole WJ: Double tensile twinning in a Mg-8Al-0.5Zn alloy. Journal of Microscopy 242 (1), 2011, 26-36. https://doi.org/10.1111/j.1365-2818.2010.03434.x.
37. Lou Y, Li L, Zhou J, Na L: Deformation behavior of Mg-8Al magnesium alloy compressed at medium and high temperatures. Materials Characterization 62 (3), 2011, 346-353. https://doi.org/10.1016/j.matchar.2011.01.004.
38. Syam P, Kondaiah V, Akhil K, Kumar V, Nagamani B, Jhansi K, Dumpala R, Venkateswarlu B, Ratna S: Effect of heat treatment on microstructure, microhardness and corrosion resistance of ZE41 Mg alloy. Koroze a ochrana materialu 63, 2019, 79-85. https://doi.org/10.2478/kom-2019-0010.
39. Jia H, Feng X, Yang Y: Influence of solution treatment on microstructure, mechanical and corrosion properties of Mg-4Zn alloy. Journal of Magnesium and Alloys 3 (3), 2015, 247-252. https://doi.org/10.1016/j.jma.2015.08.006.
40. Humphreys FJ: *Recrystallization of single-phase alloys*. In: Recrystallization and related annealing phenomena. 2nd edn. Elsevier, Australia, 2004, 215-267.
41. Han K, Hirth J, Embury J: Modeling the formation of twins and stacking faults in the ag-cu system. Acta materialia 49 (9), 2001, 1537-1540. https://doi.org/10.1016/S1359-6454(01)00057-X.
42. Duly D, Simon J.P, Brechet Y: On the competition between continuous and discontinuous precipitations in binary Mg-Al Alloys. Acta Metallurgica et Materialia 43(1), 1995, 101-106. https://doi.org/10.1016/0956-7151(95)90266-X.
43. Celotto S: TEM study of continuous precipitation in Mg-9wt%Al-1wt%Zn Alloy. Acta Materialia 48(8), 2000, 1775-1787. https://doi.org/10.1016/S1359-6454(00)00004-5.
44. Braszczyńska-Malik K.N, Kamieniak J: Non-standard heat treatment of cast AZ91 magnesium alloy. Archives of Foundry Engineering 8(1), 2008, 31-34.
45. Epler M: Structures by Precipitation from Solid Solution. In: Vander Voort GF (ed) Metallography and Microstructures, vol 9. ASM International, 2004, 134-139. https://doi.org/10.31399/asm.hb.v09.a0003731.
46. Mendis CL, Hono, K.: *Understanding precipitation processes in magnesium alloys*. In Fundamentals of Magnesium Alloy Metallurgy, Pekguleryuz MO, Kainer KU, Arslan KA, eds., Woodhead Publishing, 2013, 125-151. https://doi.org/10.1533/9780857097293.125.
47. Manna I: Discontinuous reactions in solids. International Materials Reviews 46 (2), 2013, 53-91. https://doi.org/10.1179/095066001101528402.
48. Łabanowski J, Olkowski T: Effect of microstructure on mechanical properties of BA1055 bronze castings. Archives of Foundry Engineering 14 (2), 2014, 73-78. https://doi.org/10.2478/afe-2014-0040.
49. Braszczyńska-Malik K: *Precipitates of Gamma-$Mg_{17}Al_{12}$ Phase in Mg-Al Alloys*. In: Magnesium Alloys-Design, Processing and Properties. IntechOpen, 2011. https://doi.org/10.5772/13115.
50. Crawley AF, Milliken KS: Precipitate morphology and orientation relationships in an aged Mg-9% Al-1% Zn-0.3% Mn alloy. Acta Metallurgica 22 (5), 1974, 557-562. https://doi.org/10.1016/0001-6160(74)90152-7.
51. Nie JF, Xiao XL, Luo CP, Muddle BC: Characterisation of precipitate phases in magnesium alloys using electron microdiffraction. Micron 32 (8), 2001, 857-863. https://doi.org/10.1016/S0968-4328(00)00094-9.
52. Matsukawa Y: Crystallography of precipitates in metals and alloys:(2) Impact of crystallography on precipitation hardening. In: Crystallography. IntechOpen, 2019. https://doi.org/10.5772/intechopen.84273.
53. Horst E, Friedrich BLM: *Physical Metallurgy - Chapter 3*. In: Magnesium Technology, Design Data, Applications. Springer, 2006. http://doi.org/10.1007/3-540-30812-1_3.